Synthesis of Chemically Sharp Interface in $NdNiO_3/SrTiO_3$ Heterostructures

Yueying Li(李月莹)[1,2†], Xiangbin Cai(蔡祥滨)[3†], Wenjie Sun(孙文杰)[1,2], Jiangfeng Yang(杨江枫)[1,2], Wei Guo(郭维)[1,2], Zhengbin Gu(顾正彬)[1,2], Ye Zhu(朱叶)[3*], and Yuefeng Nie(聂越峰)[1,2*]

[1]*National Laboratory of Solid State Microstructures, Jiangsu Key Laboratory of Artificial Functional Materials, College of Engineering and Applied Sciences, Nanjing University, Nanjing 210093, China*
[2]*Collaborative Innovation Center of Advanced Microstructures, Nanjing University, Nanjing 210093, China*
[3]*Department of Applied Physics, Research Institute for Smart Energy, The Hong Kong Polytechnic University, Hong Kong 999077, China*

(Received 11 February 2023; accepted manuscript online 29 May 2023)

The nickel-based superconductivity provides a fascinating new platform to explore high-T_c superconductivity. As the infinite-layer nickelates are obtained by removing the apical oxygens from the precursor perovskite phase, the crystalline quality of the perovskite phase is crucial in synthesizing high quality superconducting nickelates. Especially, cation-related defects, such as the Ruddlesden–Popper-type (RP-type) faults, are unlikely to disappear after the topotactic reduction process and should be avoided during the growth of the perovskite phase. Herein, using reactive molecular beam epitaxy, we report the atomic-scale engineering of the interface structure and demonstrate its impact in reducing crystalline defects in Nd-based nickelate/$SrTiO_3$ heterostructures. A simultaneous deposition of stoichiometric Nd and Ni directly on $SrTiO_3$ substrates results in prominent Nd vacancies and Ti diffusion at the interface and RP-type defects in nickelate films. In contrast, inserting an extra [NdO] monolayer before the simultaneous deposition of Nd and Ni forms a sharp interface and greatly eliminates RP-type defects in nickelate films. A possible explanation related to the polar discontinuity is also discussed. Our results provide an effective method to synthesize high-quality precursor perovskite phase for the investigation of the novel superconductivity in nickelates.

DOI: 10.1088/0256-307X/40/7/076801

The recently discovered superconductivity in hole-doped infinite-layer nickelate $Nd_{1-x}Sr_xNiO_2$ films, as an analogue of cuprates, has attracted much research attention, providing new opportunities to investigate the underlying physics of high-T_c superconductivity (HTSC).[1–11] Due to the instability of +1 valence state of nickel, the infinite-layer nickelate is hard to grow directly. Instead, the precursor phase, perovskite nickelate (Nd,Sr)NiO_3, is synthesized first and soft-chemically reduced subsequently to the infinite-layer phase (Nd,Sr)NiO_2 with reductive agents, such as sodium hydride.[12,13] Though great advances have been made, it still remains challenging to eliminate lattice defects during the synthesis of superconducting nickelates.[14–16] In the soft-chemical reduction process, only the oxygen content in the oxide is changed while the cation structural framework remains unchanged. That is, the cation-related defects formed during the growth of perovskite phase can persist after the reduction, such as the Ruddlesden–Popper-type (RP-type) stacking fault, a common and influential defect in the superconducting nickelates.[14,15] Therefore, the quality of the precursor phase has direct impacts on the quality of infinite-layer phase, and the cation-related defects should be avoided in advance during the growth process.

To optimize the growth of perovskite-phase films, many factors should be taken into account precisely, such as the stoichiometry,[17] growth pressure,[18] and laser fluence.[14,19] In addition, the interface chemical composition also matters. The issue regarding interface effects deserves especial attention in nickelates, given that the superconductivity is hitherto only present in the infinite-layer nickelate films while absent in the bulk- and powdered-form samples without the existence of interface.[20–22] When observed in the $[100]_p$ projection, perovskite nickelate $NdNiO_3$ consists of alternating $(NdO)^+$ and $(NiO_2)^-$ layers [Fig. S1(a) in the Supplementary Materials], which is usually grown on the (001)-oriented $SrTiO_3$ (STO) substrates with $(SrO)^0$ and $(TiO_2)^0$ layers, leading to the polar discontinuity at the polar/nonpolar interface. The resulting polar catastrophe will affect the quality of nickelate films on STO substrates, including the emergence of secondary phases with Ni^{2+} valence state,[23,24] the rough surface morphology,[25] formation of oxygen vacancies,[26] and other defects.[27] The precise control of interface chemistry, especially the first atomic layer, has been demonstrated to contribute to the lattice structure in some other nonpolar/polar heterostructures such as the $SrTiO_3/LaAlO_3$,[28] $SrVO_3/LaAlO_3$,[29]

†These authors contributed equally to this work.
*Corresponding authors. Email: yezhu@polyu.edu.hk; ynie@nju.edu.cn
© 2023 Chinese Physical Society and IOP Publishing Ltd

and $SrTiO_3/CeO_2$.[30] Nevertheless, similar investigations on nickelate films are still lacking.

In this work, utilizing the reactive molecular beam epitaxy (MBE), we optimize the crystalline quality of Nd-based nickelate/$SrTiO_3$ heterostructures by engineering the interface chemical composition with atomic precision. The defective interface with Nd vacancies, cation diffusion and RP-type stacking faults are observed in $NdNiO_3$ (NNO) films grown directly on TiO_2-terminated $SrTiO_3$ substrates. The deposition of one excess [NdO] atomic layer prior to the codeposition of Nd and Ni shows effective suppression of the Nd vacancies and Ti diffusion, which is also beneficial to reduce the lattice defects and to improve the crystalline quality. Further impacts of the interface engineering on the Sr-doped nickelate and the superconductivity are also revealed. The secondary phase with dense RP-type faults is dominated in (Nd,Sr)NiO_3 films without depositing excess [NdO] at the interface, resulting in a highly insulating behavior of the reduced phase instead of the superconductivity. Our work provides an effective route to modulate the interface structure between polar nickelate films and non-polar $SrTiO_3$ substrates, which significantly enhances the quality of nickelate films.

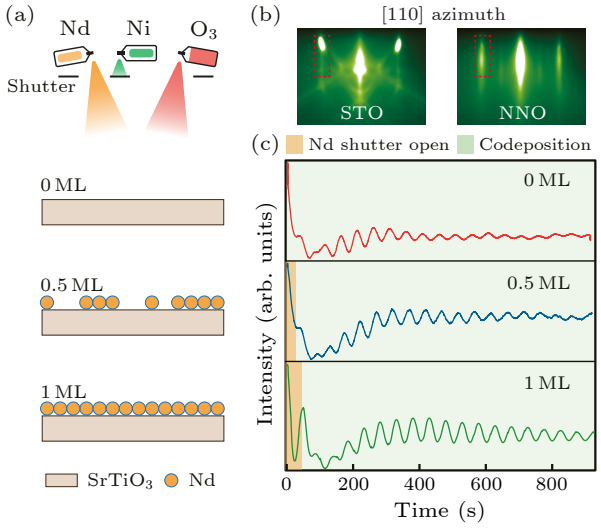

Fig. 1. (a) Schematic diagrams of MBE growth and the interface engineering. The Nd and Ni beams are controlled separately by their shutters. Different doses of the inserted extra [NdO] before the codeposition of $NdNiO_3$ are shown and named by 0 ML, 0.5 ML, and 1 ML, respectively. (b) RHEED patterns of $SrTiO_3$ (STO) substrate (left panel) and $NdNiO_3$ (NNO) film (right panel) of the 1 ML sample. (c) RHEED intensity oscillations of 18-u.c.-$NdNiO_3$ films of different interface conditions, which are obtained by monitoring the 11 diffraction spots marked by the red dashed rectangles in (b) during the growth. The yellow areas indicate the growth of excess [NdO] monolayer where the Nd shutter is open while Ni shutter closed, and the green areas indicate the codeposition of the $NdNiO_3$ where the Nd and Ni shutters are both kept open simultaneously.

The $NdNiO_3$ and (Nd,Sr)NiO_3 films were epitaxially grown on the TiO_2-terminated (001)-oriented $SrTiO_3$ single-crystalline substrates using a DCA R450 MBE system equipped with the *in situ* reflection high-energy electron diffraction (RHEED). An electron beam of 15 keV energy was utilized during the RHEED measurements. $SrTiO_3$ substrates were etched in buffered HF acid for about 70 s and annealed in flowing pure oxygen at 1000 ℃ for 80 min before growth to obtain TiO_2-terminated step-and-terrace surface.[31] The films were grown at 550–650 ℃ (measured by a thermocouple) and under an oxidant (distilled ozone) background pressure of $\sim 4.0 \times 10^{-6}$ Torr. The doping level of Sr in (Nd,Sr)NiO_3 is 20%. The nominal beam flux ratio of Nd and Ni was measured by the quartz crystal microbalance roughly and optimized precisely to meet the stoichiometry.[15] In the MBE growth of $NdNiO_3$ films, the doses of Nd and Ni are controlled independently by their respective shutters, as shown in Fig. 1(a). As a result, the film could be grown via either shuttered method (Nd and Ni deposited alternatively) or co-deposition method (Nd and Ni deposited simultaneously), which is convenient for the atomically precise modulation of the interface structures. In this work, we utilize the co-deposition method to grow the $NdNiO_3$ layer and to modulate the interface with pre-depositing the excess [NdO] layer using the shuttered method. The film crystalline structure was examined by XRD using a Bruker D8 Discover diffractometer with Cu K_α source. The specimens for the cross-sectional scanning transmission electron microscopy (STEM) were prepared by focused ion beam (FIB) techniques. Atomic-resolution annular dark-field (ADF) images and energy-dispersive x-ray spectroscopy (EDS) maps were acquired on the JEOL JEM ARM 200F outfitted with an ASCOR fifth-order probe corrector.

Figure 2 shows the analysis of atomic structure of the $NdNiO_3$ films directly grown on the TiO_2-terminated $SrTiO_3$ in stoichiometry without any interface engineering. The atomic-resolution EDS map reveals the chemical distributions of Nd (deep blue), Ni (green), Sr (light blue), and Ti (red) elements across the $NdNiO_3/SrTiO_3$ interface. The corresponding integrated concentration profiles are also shown in Fig. 2(a). The intensity of Nd has a prominent reduction at the interface layer compared to other layers within the film, that is, considerable Nd vacancies form at the interface. In addition, Ti atoms diffuse to the first $NdNiO_3$ layer and occupy part of Ni sites, as marked by the red arrow. The extent of Ti atom diffusion in our observation is comparable to the previous report.[32] Other elements show little diffusion across the interface. Meanwhile, the crystalline quality of $NdNiO_3$ films based on the rough interface is examined by the ADF-STEM image. There are some defective regions marked by the red rectangles in Fig. 2(b). Within those regions, the contrast between Nd and Ni atoms are reduced, implying the possible presence of the RP-type faults. To further explore the defects, Fourier filtering is employed, which is usually adopted to analyze the dislocation defects.[33] Figures 2(c) and 2(d) show the Fourier-filtered images from (001) and (100) reflections of the ADF-STEM images, respectively. Here, stacking faults with the half-atomic-layer displacement along c axis are indicated by the white arrows in

Fig. 2(c), which are consistent with the defective regions in Fig. 2(b). Edge dislocations with extra vertical atomic layers inserted above or below are also pointed in Fig. 2(d). Combining these two features, we can realize that the defective regions in the films are most likely to be RP-type stacking faults.

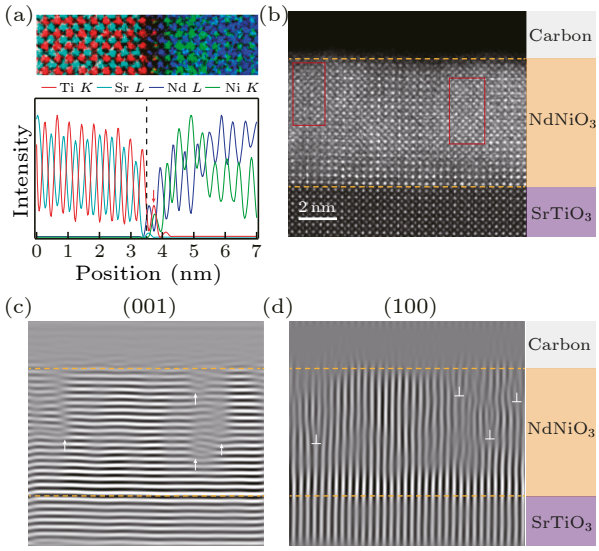

Fig. 2. (a) EDS mapping and corresponding line profiles of the 0 ML sample. The intensities of all the spectra are normalized for clarity. The position of the $NdNiO_3/SrTiO_3$ interface is indicated by the dashed black line. The red arrow indicates the diffused Ti atoms. (b) Cross-sectional ADF-STEM image of the 0 ML sample. The yellow dashed lines represent the interface between the $NdNiO_3$ film and the $SrTiO_3$ substrate and that between the film and carbon. [(c), (d)] Fourier-filtered images using (001) (c) and (100) (d) reflections corresponding to the ADF image in (b). Scale bar: 2 nm.

The polar discontinuity between $NdNiO_3$ and $SrTiO_3$ is commonly considered as the driving force of the interface reconstruction reported both theoretically and experimentally.[32,34] Likewise, the results of our experiment indicate that the alternating $[NdO]^+$ and $[NiO_2]^-$ layers with polarity are less inclined to stack spontaneously on the nonpolar layers of the $SrTiO_3$ substrate. The formation of Nd vacancies is a possible way of interface reconstruction, which could reduce the polarity of the interfacial [NdO] layer. Therefore, excess Nd may be in demand to form the complete [NdO] layer and to enhance the interface quality. Herein, the [NdO] monolayer (ML) is deposited before the codeposition of Nd and Ni to complete the interfacial [NdO] layer, forming a polar terminated surface on the nonpolar substrate prior to $NdNiO_3$ growth. As shown in Fig. 1(a), various dosages of predeposited [NdO] monolayer are referred as 0 ML, 0.5 ML, and 1 ML, respectively. The 1 ML represents the insertion of one full layer of [NdO] on the substrate surface and 0.5 ML represents half layer. It is noted that the films were grown under the identical growth condition except for the interface and on the same day to minimize the possible variation in growth parameters, such as beam fluxes and background pressure. The pre-deposition of [NdO] monolayer can be controlled based on the *in situ* RHEED, which is commonly employed to *in situ* monitor the growth process and provide the accurate deposition time. As shown in Fig. 1(c), continuous RHEED intensity oscillations of the (11) diffractions marked in Fig. 1(b) are observed during the $NdNiO_3$ growth in each case. During the deposition of [NdO] monolayer on the TiO_2-terminated $SrTiO_3$, the RHEED intensity decreases first and then increases to the maximum, the emergence of which indicates that one full [NdO] monolayer has been deposited. Note that the incident angle of the electron beam is related to the mean inner potential and consequently influences the trend of RHEED intensity.[35] Hence, it is necessary to find the appropriate incident angle at which the intensity maximum emerges at the end of [NdO] monolayer growth.[36] After the [NdO] monolayer growth, the Nd and Ni shutters were opened together to grow the $NdNiO_3$ film subsequently. The thickness of the co-deposited $NdNiO_3$ films is controlled to be nearly identical [18 unit cells (u.c.)] by RHEED intensity oscillations, the period of which corresponds to the growth of one-unit-cell $NdNiO_3$.

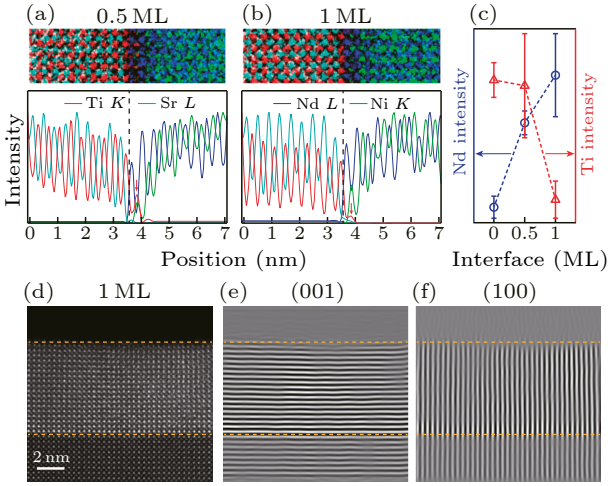

Fig. 3. [(a), (b)] EDS mapping with corresponding line profiles of the 0.5 ML (a) and 1 ML (b) samples. (c) The evolution of intensities of the interface Nd layer and the diffused Ti at the interface under different interface conditions. The error bars represent the fitting error of the line profiles. (d)–(f) Cross-sectional ADF-STEM image (d) and corresponding Fourier-filtered images using (001) (e) and (100) (f) reflections of the 1 ML sample. Scale bar: 2 nm.

The modulated interface structure of the samples with the pre-deposition of [NdO] layer is also revealed by atomic-resolution EDS. As shown in Figs. 3(a) and 3(b), the Nd vacancies have been reduced after interface engineering reflected by the increasing intensity of interface Nd. From 0.5 ML to 1 ML, the interface [NdO] atomic layer is completed gradually. Simultaneously, the extent of Ti diffusion remains virtually unchanged in the 0.5 ML sample but is substantially suppressed in the 1 ML sample, consistent with the minimized Nd vacancies. For clarity, the evolution of Nd intensity of the interface layer along

with the diffused Ti intensity on the interface conditions has been extracted from the peaks of first-unit-cell $NdNiO_3$ in their respective line profiles and plotted in Fig. 3(c). The error bars denote the fitting error of the intensity peaks. In the perovskite oxide ABO_3, the migration of smaller B-site atoms through the larger A-site vacancies is under expectation, such as in $SrTiO_3$ as reported previously.[37,38] It can be inferred that the coupled existence and disappearance of Nd vacancies and Ti diffusion in our experiments are expected because the diffused Ti atoms can migrate through the Nd-vacancy channel, implying that the suppression of the Nd vacancies is key to rehabilitating the interface structure. Hence, the chemically sharp and abrupt interface with the atomic structure of NdO/TiO_2 could be produced forcedly when excess Nd is provided at the interface. Moreover, the gradually filled Nd vacancies in the 0.5 ML and 1 ML samples suggest that the dosage of excess Nd is related to the degree of Nd vacancies, which can also be interpreted as the different degree of compensation for polar discontinuity by the Nd vacancies. Additionally, the crystalline quality of the entire film is also enhanced as confirmed by STEM. A sharp contrast between Nd and Ni atoms is observed as shown in Fig. 3(d). In Figs. 3(e) and 3(f), the Fourier-filtered images show well-ordered atomic layers in the film without obvious dislocations. That is, the RP-type faults are less likely to form in films with the sharp interface.

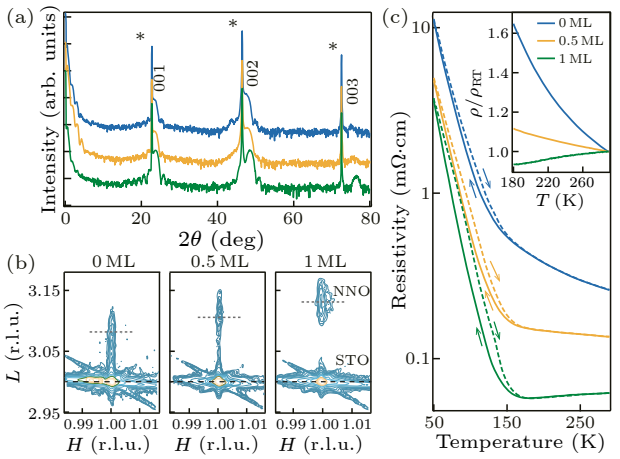

Fig. 4. (a) XRD 2θ–ω patterns of $NdNiO_3$ films under different interface conditions along [00l] direction. The asterisks denote the peaks of the STO substrate. The curves are offset vertically for clarity. (b) Corresponding RSM images around the STO (103) peak for $NdNiO_3$ films. The dashed lines indicate the peak positions. (c) Corresponding temperature-dependent resistivity of the $NdNiO_3$ films. The solid and dashed curves represent the cooling and warming processes, respectively. Inset: the $\rho(T)$ before the transition normalized by the resistivity at room temperature (ρ_{RT}) shown in linear scale.

Additionally, the XRD patterns and transport properties are studied to investigate the macroscopic impact of the interface engineering. As shown in Fig. 4(a), the 2θ–ω scans with clear (00l) peaks of 1 ML samples further demonstrate the higher macroscopic crystalline quality, while the weaker (003) peak of 0 ML and 0.5 ML samples indicates the lower crystalline quality. It is noted that the RP-type faults only exist in nanoscale regions in our films, so it cannot be identified in XRD scans for the lack of long-range order. The peak position of $NdNiO_3$ in the 2θ–ω scans exhibits an obvious shift along with the interface engineering of excess [NdO] monolayer deposition, indicating that the corresponding out-of-plane lattice constant c decreases gradually. The epitaxial growth without lattice relaxation is confirmed by reciprocal space mapping (RSM) images in all three samples, as shown in Fig. 4(b). Thus, the larger c can reflect the possible lattice expansion due to the defects in the samples without interface engineering. The trend of out-of-plane lattice constant c is more intuitive in the RSM images. The XRD results demonstrate the effective crystallinity improvement of $NdNiO_3$ films after the interface engineering, in agreement with the microscopic observations. The intrinsic metal-insulator transition (MIT) behavior resulting from the charge disproportionation together with the hysteresis loop is prototypical in $NdNiO_3$ films.[39] Figure 4(c) shows the transport properties of the corresponding $NdNiO_3$ films under different interface conditions. In the 0 ML sample, the insulating behavior starting from room temperature to the lowest temperature is observed, consistent with the inferior crystalline quality. With the interface engineering, the insulating behavior becomes weaker with lower resistivity in the 0.5 ML sample and the MIT behavior revives finally in the 1 ML sample. The increase in conductivity together with the gradually enhanced thermal hysteresis verifies the improvement of the overall crystallinity influenced by the interface condition. It is known that the perovskite $NdNiO_3$ is the precursor phase of the infinite-layer nickelate. Since the infinite-layer phase is obtained via removing apical oxygen atoms of the NiO_6 octahedra, the lattice quality of the precursor phase is crucial for the topotactic reduction. As shown in Fig. S2 in the Supplementary Materials, the sample reduced from the 0 ML precursor phase with no inserted [NdO] shows little sign of infinite-layer phase in 2θ–ω scan, which is highly insulating with resistivity beyond the measurement limit. Instead, the (00l) diffraction peaks indicating prototypical infinite-layer phase can be detected in the samples with insertion of the interface [NdO] layer. However, only the $NdNiO_2$ sample with one [NdO] monolayer shows the metallic behavior which is corresponding to the self-doping effect in $NdNiO_2$, whereas the 0.5 ML sample is still insulating. It is thus clear that the interface engineering is also important to synthesize high-quality infinite-layer nickelate films.

Furthermore, we conducted the interface engineering in Sr-doped nickelate films (Fig. 5). XRD pattern of the (Nd,Sr)NiO_3 film without interfacial [NdO] monolayer (0 ML) shows a strong peak near STO (002) whose position is below 48° and a very weak peak near STO (001), demonstrating the formation of a secondary phase consisting of dense RP-type faults.[14] Pre-deposition of one [NdO] monolayer significantly enhances the crystallinity of (Nd,Sr)NiO_3 phase. Sharp (00l) diffraction peaks are

detected with correct position of (002) peak at 48.317°. The metallic behavior is also consistent with previous reports. After the topotactic reduction, similar results for the reduced phase were obtained as the undoped compound. The infinite-layer phase exhibiting superconductivity can be obtained from the 1 ML samples, while the 0 ML sample shows neither infinite-layer phase nor superconductivity owing to the dense defects. The resistivity of the 0 ML (Nd,Sr)NiO_2 sample runs out of the measurement limit. Hence, the interface engineering via predeposition of one full [NdO] monolayer plays a critical role on the crystallinity of Sr-doped $NdNiO_3$ and thus crucial to achieving superconductivity in the infinite-layer nickelate.

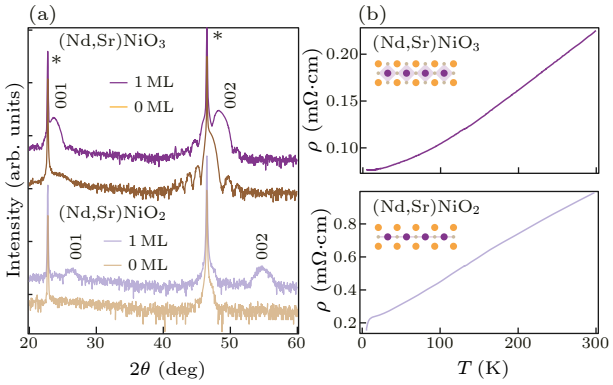

Fig. 5. XRD 2θ–ω patterns along [00l] direction (a) and temperature-dependent resistivity (b) of (Nd,Sr)NiO_3 and (Nd,Sr)NiO_2 films obtained under different interface conditions. The resistivity of both 0 ML and 0 ML samples runs out of the measurement limit. Insets: schematic crystal structures of perovskite and infinite-layer phases.

Our work provides a specific case to show the critical role of an interfacial [NdO] layer at the beginning of the film growth for the quality of nickelate films. It should also be noted that the exact initial interfacial composition of nickelate films could be sensitive to the growth techniques and the substrate surface termination. As such, different amounts of intentional deposition of initial interfacial [NdO] layer in different cases could be drastically different. In summary, we provide an effective interface engineering strategy in this work to obtain chemically sharp interface between $NdNiO_3$ and $SrTiO_3$ and avoid resultant RP-type stacking faults in $NdNiO_3$ films. The critical impacts of the interface structure on the overall nickelate film quality and the superconductivity are demonstrated. Our findings are instructive for growth of high-quality nickelate films with sharp interface on nonpolar $SrTiO_3$ substrates, aiding in syntheses of high-quality superconducting nickelates.

Acknowledgements. This work was supported by the National Key Projects for Research and Development of China (Grant No. 2022YFA1402502 and 2021YFA1400400), the National Natural Science Foundation of China (Grant No. 11861161004), the Fundamental Research Funds for the Central Universities (Grant No. 0213–14380221), the Research Grants Council of Hong Kong (Grant No. N_PolyU531/18), and the Hong Kong Polytechnic University (Grant No. ZVRP).

References

[1] Li D F, Lee K, Wang B Y, Osada M, Crossley S, Lee H R, Cui Y, Hikita Y, and Hwang H Y 2019 *Nature* **572** 624
[2] Gu Q Q and Wen H H 2022 *Innovation* **3** 100202
[3] Mitchell J F 2021 *Front. Phys.* **9** 813483
[4] Li D F, Wang B Y, Lee K, Harvey S P, Osada M, Goodge B H, Kourkoutis L F, and Hwang H Y 2020 *Phys. Rev. Lett.* **125** 027001
[5] Zeng S W, Tang C S, Yin X, Li C, Li M, Huang Z, Hu J, Liu W, Omar G J, Jani H, Lim Z S, Han K, Wan D, Yang P, Pennycook S J, Wee A T S, and Ariando A 2020 *Phys. Rev. Lett.* **125** 147003
[6] Pan G A, Ferenc S D, LaBollita H, Song Q, Nica E M, Goodge B H, Pierce A T, Doyle S, Novakov S, Córdova C D, N'Diaye A T, Shafer P, Paik H, Heron J T, Mason J A, Yacoby A, Kourkoutis L F, Erten O, Brooks C M, Botana A S, and Mundy J A 2022 *Nat. Mater.* **21** 160
[7] Tam C C, Choi J, Ding X, Agrestini S, Nag A, Wu M, Huang B, Luo H, Gao P, García-Fernández M, Qiao L, and Zhou K J 2022 *Nat. Mater.* **21** 1116
[8] Lu H, Rossi M, Nag A, Osada M, Li D F, Lee K, Wang B Y, Garcia-Fernandez M, Agrestini S, Shen Z X, Been E M, Moritz B, Devereaux T P, Zaanen J, Hwang H Y, Zhou K J, and Lee W S 2021 *Science* **373** 213
[9] Gu Q Q, Li Y Y, Wan S Y, Li H Z, Guo W, Yang H, Li Q, Zhu X Y, Pan X Q, Nie Y F, and Wen H H 2020 *Nat. Commun.* **11** 6027
[10] Wang B Y, Li D F, Goodge B H, Lee K, Osada M, Harvey S P, Kourkoutis L F, Beasley M R, and Hwang H Y 2021 *Nat. Phys.* **17** 473
[11] Li D F 2021 *Sci. Sin.-Phys. Mech. Astron.* **51** 047405 (in Chinese)
[12] Hayward M A, Green M A, Rosseinsky M J, and Sloan J 1999 *J. Am. Chem. Soc.* **121** 8843
[13] Kawai M, Inoue S, Mizumaki M, Kawamura N, Ichikawa N, and Shimakawa Y 2009 *Appl. Phys. Lett.* **94** 082102
[14] Lee K, Goodge B H, Li D F, Osada M, Wang B Y, Cui Y, Kourkoutis L F, and Hwang H Y 2020 *APL Mater.* **8** 041107
[15] Li Y Y, Sun W J, Yang J F, Cai X B, Guo W, Gu Z B, Zhu Y, and Nie Y F 2021 *Front. Phys.* **9** 719534
[16] Osada M, Wang B Y, Goodge B H, Harvey S P, Lee K, Li D F, Kourkoutis L F, and Hwang H Y 2021 *Adv. Mater.* **2021** 2104083
[17] Yamanaka T, Hattori A N, Pamasi L N, Takemoto S, Hattori K, Daimon H, Sato K, and Tanaka H 2019 *ACS Appl. Electron. Mater.* **1** 2678
[18] Obradors X, Paulius L M, Maple M B, Torrance J B, Nazzal A I, Fontcuberta J, and Granados X 1993 *Phys. Rev. B* **47** 12353
[19] Breckenfeld E, Chen Z, Damodaran A R, and Martin L W 2014 *ACS Appl. Mater. Interfaces* **6** 22436
[20] Wang B X, Zheng H, Krivyakina E, Chmaissem O, Lopes P P, Lynn J W, Gallington L C, Ren Y, Rosenkranz S, Mitchell J F, and Phelan D 2020 *Phys. Rev. Mater.* **4** 084409
[21] Li Q, He C P, Si J, Zhu X Y, Zhang Y, and Wen H H 2020 *Commun. Mater* **1** 16
[22] Puphal P, Wu Y M, Fürsich K, Lee H, Pakdaman M, Bruin J A N, Nuss J, Suyolcu Y E, van Aken P A, Keimer B, Isobe M, and Hepting M 2021 *Sci. Adv.* **7** eabl8091
[23] Detemple E, Ramasse Q M, Sigle W, Cristiani G, Habermeier H U, Benckiser E, Boris A V, Frano A, Wochner P, Wu M, Keimer B, and van Aken P A 2011 *Appl. Phys. Lett.* **99** 211903

[24] Middey S, Rivero P, Meyers D, Kareev M, Liu X, Cao Y, Freeland J W, Barraza-Lopez S, and Chakhalian J 2014 *Sci. Rep.* **4** 6819
[25] Liu J, Kareev M, Prosandeev S, Gray B, Ryan P, Freeland J W, and Chakhalian J 2010 *Appl. Phys. Lett.* **96** 133111
[26] Tung I C, Luo G, Lee J H, Chang S H, Moyer J, Hong H, Bedzyk M J, Zhou H, Morgan D, Fong D D, and Freeland J W 2017 *Phys. Rev. Mater.* **1** 053404
[27] Yang H F, Liu Z T, Fan C C, Yao Q, Xiang P, Zhang K L, Li M Y, Liu J S, and Shen D W 2016 *AIP Adv.* **6** 085115
[28] Kim D W, Kim D H, Kang B S, Noh T W, Lee D R, and Lee K B 1999 *Appl. Phys. Lett.* **74** 2176
[29] Kim D W, Kim D H, Noh T W, Char K, Park J H, Lee K B, and Kim H D 2000 *J. Appl. Phys.* **88** 7056
[30] Yamada T, Kiguchi T, Wakiya N, Shinozaki K, and Mizutani N 2003 *MRS Online Proc. Library* **747** 17
[31] Kawasaki M, Takahashi K, Maeda T, Tsuchiya R, Shinohara M, Ishiyama O, Yonezawa T, Yoshimoto M, and Koinuma H 1994 *Science* **266** 1540
[32] Goodge B H, Geisler B, Lee K, Osada M, Wang B Y, Li D, Hwang H Y, Pentcheva R, and Kourkoutis L F 2023 *Nat. Mater.* **22** 466
[33] Ikuhara Y H, Gao X P, Huang R, Fisher C A J, Kuwabara A, Moriwake H, and Kohama K 2014 *J. Phys. Chem. C* **118** 19540
[34] He R, Jiang P H, Lu Y, Song Y D, Chen M X, Jin M L, Shui L L, and Zhong Z C 2020 *Phys. Rev. B* **102** 035118
[35] Sun H Y, Mao Z W, Zhang T W, Han L, Zhang T T, Cai X B, Guo X, Li Y F, Zang Y P, Guo W, Song J H, Ji D X, Gu C Y, Tang C, Gu Z B, Wang N, Zhu Y, Schlom D G, Nie Y F, and Pan X Q 2018 *Nat. Commun.* **9** 2965
[36] Haeni J H, Theis C D, and Schlom D G 2000 *J. Electroceram.* **4** 385
[37] Mizoguchi T, Takahashi N, and Lee H S 2011 *Appl. Phys. Lett.* **98** 091909
[38] Gömann K, Borchardt G, Gunhold A, Maus-Friedrichs W, and Baumann H 2004 *Phys. Chem. Chem. Phys.* **6** 3639
[39] Catalan G, Bowman R M, and Gregg J M 2000 *Phys. Rev. B* **62** 7892